Unsteady Aerodynamic and Stall Effects on Helicopter Rotor Blade Airfoil Sections

JAAN LIIVA*
The Boeing Company, Vertol Division, Philadelphia, Pa.

Oscillatory tests in pitch and in vertical translation were performed on symmetrical and cambered airfoils, at full-scale Reynolds numbers, to provide dynamic stall data for rotor blade analyses. The Mach number range applicable to the retreating side of the rotor disk was covered at frequencies up to the first bending and the first torsional natural frequency. A system with a torsional degree of freedom was also tested. The following key results were found: 1) The negative aerodynamic damping due to stall is highly sensitive to Mach number. 2) Negative aerodynamic damping can be encountered in large-amplitude plunging motions. 3) The maximum normal force encountered during oscillation is substantially higher than that for static stall. In addition, the flow separation process is discussed.

Nomenclature

C_M = pitching moment coefficient (pitching moment per foot span)/qc^2, positive nose-up
C_N = normal force coefficient (normal force per foot span)/qc, positive up
$C_{N\,MAX}$ = maximum C_N attained during cycle of pitch oscillation
f = frequency of oscillation, Hz
h = plunge position in semichords, positive up
k = reduced frequency, $\pi fc/v$
M = Mach number
Re = Reynolds number
$(\ )_T$ = tuned system parameter
α = instantaneous angle of attack, positive nose-up, deg
α_0 = mean angle of attack, positive nose-up, deg
$\delta\alpha$ = elastic deflection amplitude, deg
$\Delta\alpha$ = oscillatory angle of attack, deg
Δh = oscillatory plunge magnitude in semichords

Introduction

THE speed and the lifting capability of contemporary helicopters are limited by retreating blade stall which manifests itself in two ways: 1) by rapid increases in the power required with forward speed due to increased rotor drag, and 2) by rapid increases in rotor blade and control loads with forward speed. Attempts to predict the effects of blade stall by using steady-state airfoil characteristics with stall and Mach number accountability in a strip theory analysis have been unsuccessful; the onset of stall is predicted too early.

There are two recognized aerodynamic effects that can cause the differences between test and theory: radial flow and unsteady aerodynamics. Neither effect has been included in current rotor analyses. In discussing the effects of yaw on the rotor blade, Harris[1] shows that part of the discrepancy between test and theory can be eliminated by including yaw effects in the airfoil tables. Unsteady aerodynamics, the other effect, has been shown by various investigators (see bibliography in Ref. 2) to produce a stall delay which increases the maximum lift coefficient above that for static stall. In addition to this stall delay, negative aerodynamic damping can occur for pitch oscillations through stall. This negative damping is caused by the hysteresis effects of the blade pitching moment vs angle-of-attack curve, and can cause large torsional blade deflections and large control loads. The resulting blade and control stresses caused by stall can limit the flight speed of the helicopter; therefore, it is imperative that the effects of dynamic stall be fully understood. Further, these effects should be incorporated in rotor blade analyses to determine if the correlation between test and theory can be improved.

A comprehensive literature search revealed little useful oscillatory data appropriate to helicopter blade applications, and no theories that adequately predict dynamic stall effects. To provide sufficient data to stimulate the formulation of a dynamic stall theory, The Boeing Company has tested two typical helicopter rotor blade sections in sinusoidal pitching and in translating motion, matching the nonsteady aerodynamic environment existing on a helicopter rotor blade on the retreating side of the disk.

The three primary objectives of the test were as follows: 1) to determine the maximum attainable normal force coefficient at the characteristic frequencies of a rotor blade in its once-per-revolution (1/rev) motion, 2) to determine the aerodynamic damping characteristics of a rotor blade at its natural elastic bending and torsional frequencies, and 3) to investigate the detailed stalling behavior of a rotor blade airfoil in order to formulate a stall theory, and to facilitate the design of airfoils that are capable of improved operation in the unsteady aerodynamic environment of a rotor blade.

Wind-Tunnel Test Conditions

The ranges of the aerodynamic parameters required to represent the flow on the retreating side of a rotor for flight speeds up to 250 knots were determined (and are described in Ref. 2); results from that study are summarized as follows: 1) Mach number M, 0.2–0.6; 2)Reynolds number Re, 2.6–6.6 million (2-ft blade chord in standard atmosphere); 3) mean angle of attack α_0, 0–25°; 4) oscillatory angle of attack $\Delta\alpha$, 2.5–7.5°; and 5) reduced frequency k, 0.04–0.72 for pitching, 0.04–0.24 for vertical translation.

Test Facilities

In order to use the existing variable-density 1 × 3-ft wind tunnel at Boeing, a ¼-scale model of the 2-ft chord airfoil was

Presented as Paper 68-58 at the AIAA 6th Aerospace Science Meeting, New York, January 22–24, 1968; submitted January 23, 1968; revision received June 24, 1968. This research was supported in part by the U.S. Army Aviation Materiel Laboratories (USAAVLABS) under Contract DA 44-177-AMC-438(T). The substantial contributions made to the program by many individuals in the Vertol and the Airplane Divisions of The Boeing Company are gratefully acknowledged; foremost among these were F. Davenport, L. Gray, and I. Walton.

* Supervisor, Rotor and Blade Aerodynamics, Aerodynamics Research Unit.

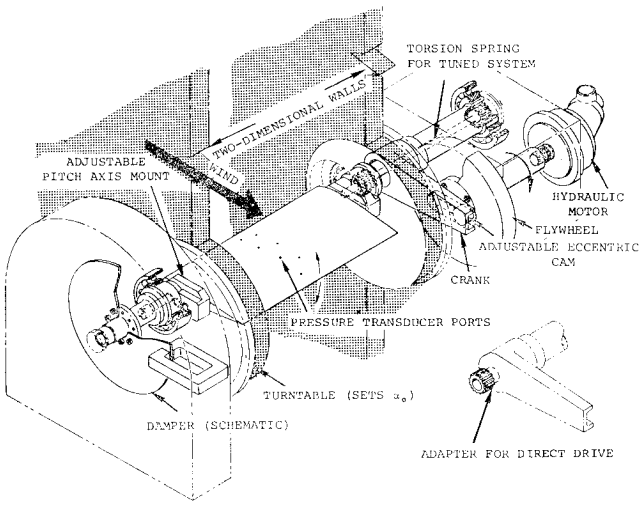

Fig. 1 Pitch oscillating mechanism.

chosen. The test section pressure and airfoil drive frequency were increased to simulate full-scale Reynolds numbers and reduced frequency. The tunnel Mach number capability was greater than the required 0.6. Three modes of testing were chosen: 1) pitch oscillation about the 25% chord, 2) vertical translation, and 3) a tuned pitch system.

To determine the stall delay, sinusoidal pitching and vertical translation were tested at frequencies corresponding to 1/rev for a helicopter rotor. The tests at higher frequencies, up to 6/rev for pitch and 2/rev for vertical translation, were aimed at measuring the negative aerodynamic damping which can cause magnification of the elastic blade motions.

In order to show the combined effects of two types of pitching motion, a tuned system was tested in which the airfoil was mounted on a torsion spring through which the background 1/rev motion was transmitted. The spring stiffness was varied to give a natural frequency from four to six times the background frequency.

The pitch oscillation mechanism is shown in Fig. 1. A flywheel with an eccentrically mounted interchangeable cam drives a crank which is connected to the airfoil by a torsion spring for the tuned system, or by an adapter for direct drive. A hydraulic motor supplies the power. An eddy-current damper was used with the tuned system for safety.

A system similar to the pitch mechanism was used for the translation tests. Airfoil end plates were required with the translating mechanism to cover slots in the tunnel walls. The tunnel wall flow separation caused by the end plates was eliminated by using wall boundary layer control.

The first airfoil chosen for testing has a modified NACA 0012 contour and is called NACA 0012 (mod). The modifications consisted of a symmetrical leading-edge fairing (corresponding to a typical anti-icing boot) and a flat sheet-metal trailing-edge extension. The resulting configuration is identical to the rotor blade section used on the CH-47A helicopter. An advanced airfoil of the type used on the CH-47B was chosen for comparison. This airfoil has a camber line similar to the NACA 230 and a thickness ratio of about 10%. A cuspate trailing edge similar to that of the first airfoil was used. The airfoil contours are shown in Fig. 2. Design characteristics and static data for both airfoils are reported by Davenport.[3]

The model airfoils were constructed of a steel center spar with sheet-metal leading and trailing edges. The span of each wing was nominally 12 in. and the chord was 6.38 in. Fourteen miniature differential-pressure transducers were used to obtain the chordwise pressure distribution. The natural frequency of the installed transducers was at least 1030 Hz with a damping factor of 0.45.

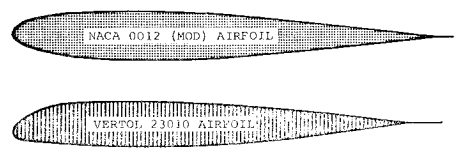

Fig. 2 Test airfoil contours.

Data Recording and Reduction System

All data, both airfoil pressure and tunnel test condition information, were recorded on two FM wide-band tape recorders. A time code and a 1/rev pulse recorded on both tapes provided tape synchronization. In addition, all parameters were recorded on an oscillograph for instant data monitoring. Included were C_N and C_M, obtained by integrating the pressures with an analog computer.

Nearly 800 individual test points were taken in a series of four tests. The total number of individual data readings was close to 10 million, since the data for 10 cycles were averaged and approximately 40 points were read per cycle. To handle this large volume of data, the recorded analog information was digitized and processed on a digital computer, using basic flight-test data reduction programs. The pressure data were integrated digitally to obtain time histories of C_N, C_M, and average cycle damping.† The flight-test data plotting system, which is integral with the data reduction system, was used to plot approximately 80% of the C_N and C_M vs α data.

Experimental Results for Pitch Oscillation Tests

The variations of the C_N-α and C_M-α loops with α_0, f, and M are presented for the Vertol 23010-1.58 airfoil. The loops for the NACA 0012 (mod) airfoil are similar in shape and will not be shown. The two airfoils will be compared in a later section on the basis of cycle damping and maximum normal force.

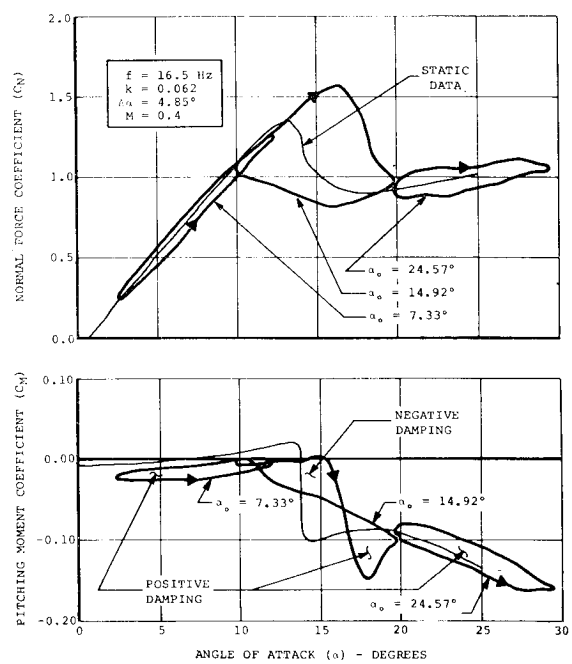

Fig. 3 Typical pitch oscillation data.

† Average cycle damping is defined as

$\oint C_M \, d\alpha$ for pitching oscillation
$\oint C_N \, dh$ for plunge oscillation

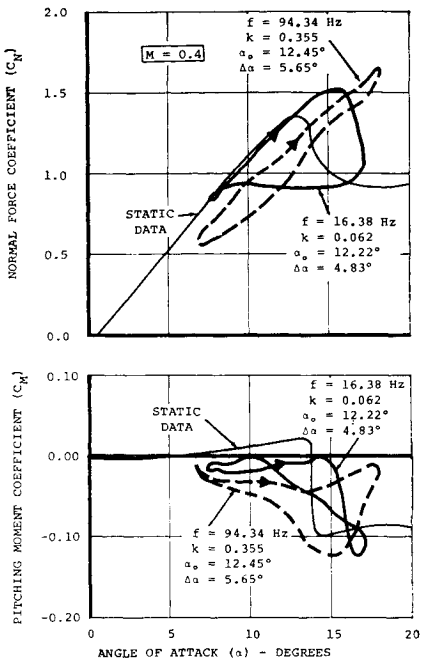

Fig. 4 Effect of frequency.

Mean Angle-of-Attack Effects

A typical set of C_N and C_M response curves is compared with steady data in Fig. 3 at values of α_0 below stall ($\alpha_0 = 7.3°$), at stall ($\alpha_0 = 14.9°$), and above stall ($\alpha_0 = 24.6°$). The model frequency, 16 Hz, is characteristic of the 1/rev motion of a rotor blade. The C_N and C_M response of the airfoil at 7.3° shows the characteristic elliptical shape predicted by unsteady airfoil theory.[4]

The area inside the C_M trace indicates the work per cycle or cycle damping. The damping is positive for a counterclockwise circuit. Areas enclosed by a clockwise circuit are damped negatively; i.e., the airfoil system extracts energy from the airstream. This can lead to an increase in the amplitude of oscillation with time for an elastic system, and is precisely the condition for flutter.

The C_N loop for $\alpha_0 = 14.9°$ shows a substantial increase in the maximum normal force above the steady stall value. The corresponding C_M trace shows almost equal areas of positive and negative damping, indicating that this test condition is neutrally damped. It is interesting to note that moment stall occurs before lift stall. The same condition was found to exist in flight-test data taken from pressure measurements by Harris and Pruyn.[5] The C_N and C_M data at $\alpha_0 = 24.6°$ represent fully separated flow with positive damping.

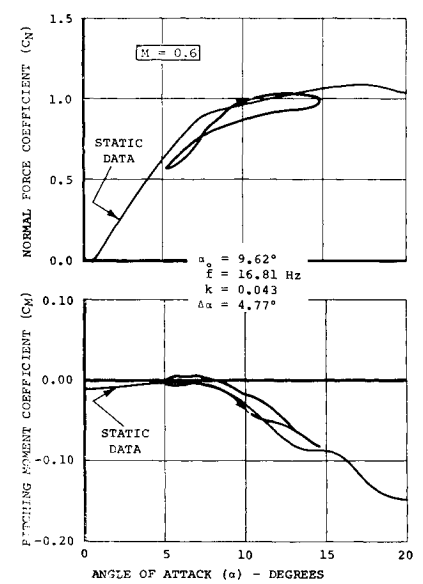

Fig. 5 Pitch oscillation data at 0.6 Mach.

Pitch Frequency Effects

Figure 4 shows the effect of increasing the pitching frequency from 1/rev to 6/rev for a test condition at stall. Three significant effects are noted:

1) The airfoil is partially stalled during the decreasing-α portion of the cycle for the higher-frequency case, even though the C_N trace shows the characteristic elliptical shape for unstalled flow. This can be confirmed by observing the sense of the C_N loop and comparing this with the $\alpha_0 = 7.3°$ data from Fig. 3. The pitching moment data at the high frequency also show definite signs of stall, both in sense and magnitude.

2) The onset of stall is significantly postponed for both the C_N and C_M traces at the increased frequency.

3) The sudden stalling apparent at the low frequency does not occur at the high frequency. This suggests that there is an upper limit to the time rate of change of circulation on the airfoil.

Mach Number Effects

The dynamic stalling behavior of an airfoil at 0.2 Mach is similar to that at 0.4 in that both positive and negative damping areas are present for the C_M trace for oscillation through stall, and therefore no data will be shown at Mach 0.2.

The data at 0.6 Mach, however, show entirely different trends from those at 0.4 Mach. This can be seen by comparing data from Figs. 3 and 5. The 0.6 Mach dynamic C_N and C_M loops follow the static line closely because the reduced frequency parameter k is very low ($k = 0.04$). The damping is positive and there are no sharp, sudden breaks in the C_N and C_M curves for both steady and oscillatory data.

This difference in behavior at 0.6 Mach was examined by comparing steady and oscillatory chordwise pressure data be-

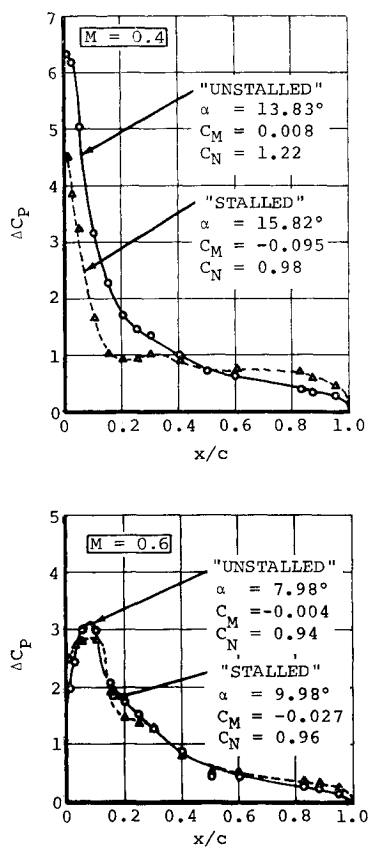

Fig. 6 Effect of Mach number on the loading distributions for the Vertol 23010 airfoil.

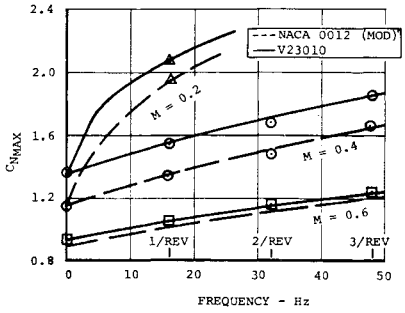

Fig. 7 Summary of $C_{N_{MAX}}$ for pitching.

low and above stall at $M = 0.4$ and at 0.6. The differences in chordwise loading below and above stall are shown for steady data in Fig. 6. The loadings corresponding to oscillatory data are similar and are therefore not shown.

At 0.4 Mach the loading is seen to be of the classical potential-flow type before stall. Above stall the distribution is altered radically and the loading is essentially constant aft of the 15% chord point, indicating flow separation.

The pressure gradient for the 0.6 Mach loadings is favorable up to the 10% chordwise location because of the supersonic expansion around the leading edge, and separation, if any, occurs aft of the shock. There is no sudden increase in the nose-down pitching moment with angle of attack because the expansion/shock system can adjust to the α changes by a slight readjustment of the leading-edge pressures and the shock location.

The negative damping at the lower Mach number is thus caused by the sudden flow separation at stall and the accompanying large, nose-down pitching moment combined with the nose-down airfoil motion after stall.

Summary of Key Results from the Pitch Oscillation Tests

Figure 7 summarizes the maximum C_N encountered during a cycle of oscillation for the symmetrical and the cambered airfoils. The cambered airfoil has a higher C_N capability over the whole frequency range because the adverse pressure gradient is decreased by nose camber.

Damping characteristics‡ for the cambered and the symmetrical airfoils are compared in Fig. 8 for a frequency of 6/rev (96 Hz model scale), a typical helicopter rotor blade first-torsion mode natural frequency. The trends with

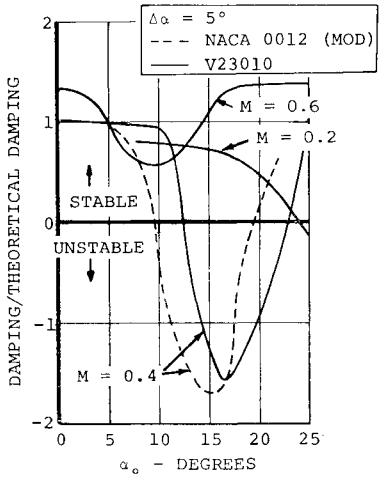

Fig. 8 Summary of pitch damping.

‡ Cycle damping is presented as a ratio to theoretical damping, derived by using the Theodorsen[4] equation for unsteady C_M in the damping equation

damping/theoretical damping = $\oint[(C_M)\ \text{test}/(C_M)\ \text{theory}]d\alpha$

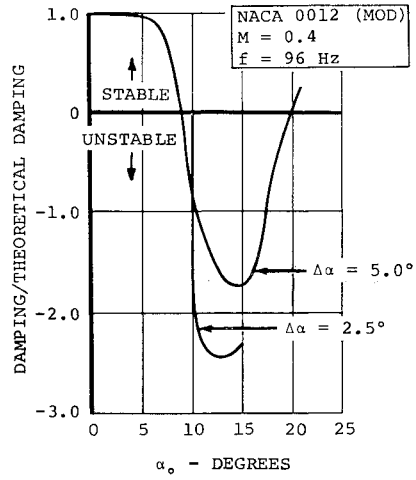

Fig. 9 Effect of oscillation amplitude.

Mach number are similar for both airfoils. The cambered section, however, is stable up to higher mean angles of attack. Maximum negative damping in magnitude and duration with mean angle of attack occurs for 0.4 Mach. At 0.6 Mach, the damping is reduced at the mean angles of attack where the steady-lift curve changes slope, but the damping does not become negative. At $M = 0.2$, the onset of negative damping is delayed to mean angles of attack substantially above the static stall.

The effect of amplitude of oscillation on cycle damping is shown in Fig. 9 for the symmetrical airfoil at 96 Hz oscillation frequency. The negative damping for the 2.5° amplitude oscillation is much larger than that for the 5° amplitude oscillation. This can be expected since stall is a highly nonlinear phenomenon.

Experimental Results for Vertical Translation Tests

C_N and C_M are plotted against h, the translation amplitude measured in semichords, in Fig. 10. Data are shown for mean angles of attack below stall, 5.02°; and at stall, 14.65°. The data at $\alpha_0 = 5.02°$ are unstalled and show the elliptical loop predicted by theory. At $\alpha_0 = 14.65°$, C_N and C_M both show stall on the downstroke. This stall is caused by an increase in the effective α due to the vector addition of plunge rate with tunnel velocity. On the upstroke, when dh/dt is positive and the effective α is reduced, the airfoil remains unstalled. This cyclic stalling results in negative damping.

Damping is proportional to the area enclosed in the C_N vs h trace, and is positive (stable) for a counterclockwise circuit. The C_M trace also shows the effects of stall. However, the total pitching moment change is only −0.12, the value for static stall.

Similar C_N and C_M loops are shown for frequency variations, Mach number changes, amplitude of oscillation changes, and

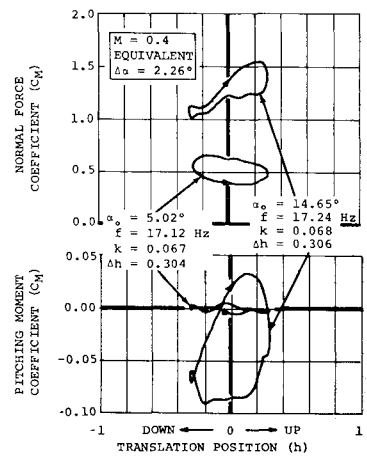

Fig. 10 Typical vertical translation data.

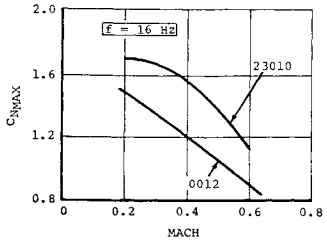

Fig. 11 Summary of $C_{N_{MAX}}$ in vertical translation.

airfoil type in Ref. 2. The significant results from the transiation tests are summarized in the next section.

Summary of Key Results from the Plunge Tests

The maximum C_N's obtained during these tests in the plunge mode for the equivalent 1/rev frequency (16-Hz model scale) are shown in Fig. 11. The higher stall angle of the 23010–1.58 airfoil is apparent in its consistent increment of 0.2 in C_N over the symmetrical section.

Figure 12 shows damping in plunge§ for the Vertol 23010–1.58 airfoil section as a function of α_0, for $M = 0.4$ and $M = 0.6$. For angles well below the static stall level, damping at $M = 0.4$ remains near the theoretical value. A loss of positive damping is apparent at 12.3°; above 15°, zero or negative damping prevails. The largest negative value occurs when α_0 is just at the stall point and the plunging motion varies the aerodynamic α just enough to cross the lift-curve discontinuity. (The C_N and C_M traces for the cycle are shown in Fig. 10.)

At 0.6 Mach the loss of damping occurs at a lower α_0, but remains at the zero damping level at higher α_0's. This is consistent with a steady C_N vs α relation in which lift has practically ceased to vary after "stall," or rather, shock separation. Both the symmetrical and the cambered airfoils exhibit these characteristics at Mach 0.6.

The damping data (not shown) for the symmetrical airfoil are similar, except that the negative damping occurs at a lower α_0 up to 0.4 Mach.

These tests were conducted at much larger Δh and at higher Mach numbers than any previous tests. This is probably why neither Halfman[6] nor Rainey[7] measured negative damping during their tests.

Tuned System Test Results

Because of the widely varying aerodynamic parameters, such as the reduced frequency and Mach number, along a rotor blade in forward flight, the stall-induced torsional oscillations of a whole blade cannot be simulated in a wind tunnel.

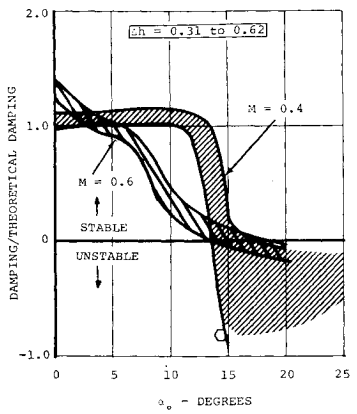

Fig. 12 Summary of damping data in vertical translation.

§ The damping data are shown as a ratio of theoretical damping, obtained by using the Theodorsen[4] relationship for C_N, i.e.,

damping/theoretical damping = $\int[(C_N)$ test$/(C_N)$ theory$]dh$

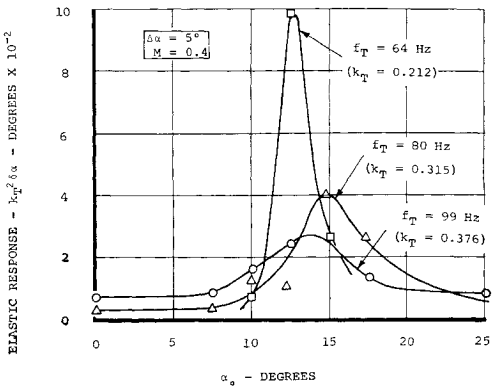

Fig. 13 Elastic system pitch response.

Another complication is the fact that the blade is not executing simple sinusoidal pitching motion at the conditions of greatest interest; rather, it is producing a combination of the 1/rev basic angle-of-attack change with varying amounts of higher-frequency elastic motions superimposed. These elastic pitching and translation deflections modify the angle of attack.

Of the elastic motions, the response of the first torsional mode is of most interest, since it can be forced to large deflections by stall effects. Therefore, the approach taken in this test was to simulate a representative blade section by spring-mounting the airfoil, which was tuned to 4, 5, and 6/rev (64-, 80-, and 96-Hz model scale), and by driving the angle of attack at 1/rev (16-Hz model scale) with the system used for the forced pitching tests. Although these model tests did not provide full-scale deflections, because the model inertia was ten times higher than the corresponding full-scale blade inertia, they provide the following: 1) The tests can predict the onset of stall-induced oscillations, because these depend on the 1/rev α variation. 2) The tests can provide data with which analytical formulations of the effects of stall on rotor blades can be checked in a dynamic system described by a simple differential equation.

The most significant result is shown in Fig. 13, where the torsional elastic response for the three tuned system frequencies f_T are compared. The response $\delta\alpha$ has been multiplied by k_T^2, to nondimensionalize the deflections with respect to the tuned frequency f_T. The increase in response is spectacular for the 4/rev system. This shows that the response to stall is highly dependent on the stiffness of the system, and that the forcing function is highly nonlinear, since a linear

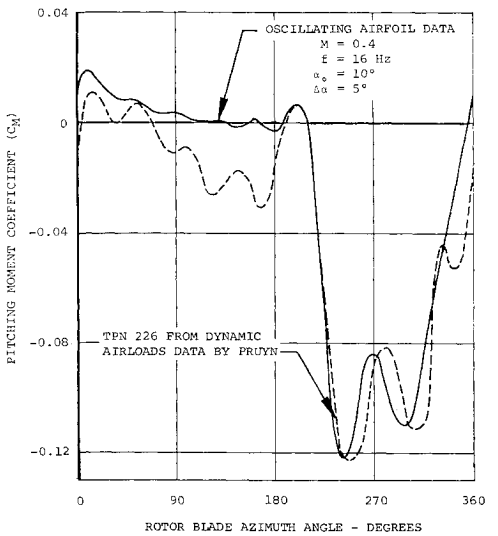

Fig. 14 Comparison of wind-tunnel and flight-test data.

system would have similar nondimensional elastic deflections for a constant forcing function.

It was also found that

1) The largest elastic response was obtained for oscillation at the stall angle for the three Mach numbers tested (0.2, 0.4, and 0.6).

2) The elastic response magnitude was independent of the driving amplitude. Driving amplitudes of 5 and 7.5° were used for these tests.

Comparison with Other Test Data and Theory

The data from these tests have been compared with theory at conditions below stall. The agreement is very good over the whole range of frequencies and Mach numbers.

C_M data from the CH-47A Dynamic Airloads Tests[8] are compared with symmetrical airfoil data from these tests in Fig. 14. The tunnel test point was chosen to represent the Mach vs α conditions on the retreating side of the rotor disk ($M = 0.4$, $\alpha_0 = 10°$, $\Delta\alpha = 5°$) and the pitch reference position has been shifted to agree with the stall point of the flight-test data. The agreement between the two tests is remarkable, both in the magnitude of the C_M change with stall and in the duration of stall. Both the wind-tunnel and the flight-test data show a partial reattachment at the 270° azimuth position followed by a further stall. The flight-test data show a 6 to 7/rev oscillation on the advancing side, which is probably elastic response. The nose-down pitching moment of the flight-test data in the 60° to 180° azimuth range may be due to the higher Mach number for that data.

Conclusions

1) The maximum normal force attained during a cycle of either pitch or vertical translation oscillation is greater than the static $C_{N\text{MAX}}$ for Mach number up to 0.6, the highest for these tests. The dynamic $C_{N\text{MAX}}$ increases with frequency.

2) There are regions of negative damping for both pitching and vertical translation motions at angles of attack near stall. The magnitude of the damping at stall is highly influenced by the amplitude of oscillation and Mach number.

3) The cambered airfoil has better aerodynamic characteristics than the symmetrical airfoil in that its $C_{N\text{MAX}}$ is greater and the inception of negative damping occurs at a higher angle of attack.

4) The effects of negative damping in pitch and plunge are strongly related to discontinuities in the static C_N and C_M curves. These discontinuities are caused by leading-edge stall. At Mach 0.6, where transonic effects eliminate leading-edge stall, damping is reduced below the potential-flow level but remains positive.

References

[1] Harris, F. D., "Spanwise Flow Effects on Rotor Performance," *Proceedings of the Symposium on Aerodynamics Problems Associated with V/STOL Aircraft,* Cornell Aeronautical Labs. and U. S. Army Aviation Material Labs., June 1966.

[2] Liiva, J. et al., "Two-Dimensional Tests of Airfoils Oscillating Near Stall," D8-0678-1,-2, Oct. 1967, The Boeing Co., Vertol Div., Philadelphia, Pa.

[3] Davenport, F. J. and Front, J. V., "Airfoil Sections for Rotor Blades—A Reconsideration," *Proceedings of the 22nd Annual National Forum,* American Helicopter Society, Inc., May 1966.

[4] Bisplinghoff, R. L., Ashley, H., and Halfman, R. L., *Aeroelasticity,* Addison-Wesley, Reading, Mass., 1955, pp. 251–281.

[5] Harris, F. D. and Pruyn, R. R., "Blade Stall—Half Fact, Half Fiction," *Proceedings of the 23rd Annual National Forum,* No. 101, American Helicopter Society, Inc., May 1967.

[6] Halfman, R. L., Johnson, H. C., and Haley, S. M., "Evaluation of High-Angle-of-Attack Aerodynamic Derivative Data and Stall-Flutter Prediction Techniques," TN 2533, Nov. 1951, NACA.

[7] Rainey, G. A., "Measurement of Aerodynamic Forces for Various Mean Angles of Attack on an Airfoil Oscillating in Pitch and on Two Finite-Span Wings Oscillating in Bending with Emphasis on Damping in the Stall," TN 3643, May 1956, NACA.

[8] Pruyn, R. R., "In-Flight Measurement of Rotor Blade Air loads, Bending Moments, and Motions, Together with Rotor Shaft Loads and Fuselage Vibration, on a Tandem Rotor Helicopter," D8-0382-4 and -5, Jan. 1967, The Boeing Co., Vertol Div., Philadelphia, Pa.